https://doi.org/10.1038/s44407-026-00066-5

Linking anthropogenic chlorine emissions to regional air quality in India

Ankit Patel[1,2] ✉, Malasani Chakradhar Reddy[1,2], Bingqing Zhang[3], Basudev Swain[4], Govindan Pandithurai[1], Meinrat O. Andreae[5,6], Scot T. Martin[7,8], Pengfei Liu[3] & Sachin S. Gunthe[1,2] ✉

India experiences severe air pollution driven by human activities. The role of anthropogenic chlorine is significant yet underexplored, with its mechanisms poorly understood and impacts largely unquantified, despite its importance in atmospheric oxidation and secondary pollutant formation. Using the GEOS-Chem chemical transport model, we quantify the impact of human-derived chlorine emissions on particulate chloride (pCl^-), particulate matter ($PM_{2.5}$), $ClNO_2$, and O_3 in the boundary layer over India. Comprehensive model simulations reveal major chlorine hotspots affecting nearly ~ 700 million people across the Indo-Gangetic Plain (IGP). The $PM_{2.5}$ concentration increases due to pCl^- formation (principally NH_4Cl). Annual mean pCl^- and $ClNO_2$ increase by 4-fold and 3-fold, respectively. Regionally and seasonally, enhancements range from $0.04 - 3.6\,\mu g\,m^{-3}$ for pCl^-, 7-273 ppt for $ClNO_2$, and -0.47-0.44 ppb for O_3 with strongest effects in autumn and winter. Compared to other polluted hotspots in the world, for example China, O_3 showed a lower sensitivity to chlorine emissions over India. Anthropogenic chlorine significantly influences India's air quality, underscoring the need to include chlorine emission inventories and chemistry in models.

India experiences severe air pollution tied to anthropogenic emissions[1–3]. Among these, anthropogenic chlorine emissions are an important yet underexplored factor influencing regional air pollution. Continental chlorine chemistry has gained significant importance in recent years due to its broad implications in tropospheric chemistry and air quality[4–6]. In polluted environments, the photolysis of reactive chlorine species (Cl_2, HCl, HOCl, ClONO, $ClNO_2$, $CHCl_3$, CH_2Cl_2) releases highly reactive Cl radicals[1,5,7,8]. These radicals drive VOC oxidation, promoting secondary organic aerosol (SOA) formation, modifying hydrocarbon, and particulate matter (PM) levels, the lifetime of trace species, and thus altering atmospheric composition and oxidative capacity[8–11]. In urban environments, nighttime chlorine chemistry plays a crucial role in modulating surface ozone (O_3) and fine particulate $PM_{2.5}$ concentrations during morning hours[3,12,13]. $NO_3^{\cdot}$, a key night-time oxidant, exists in equilibrium with dinitrogen pentoxide (N_2O_5) which undergoes heterogeneous reactions with chloride-containing aerosols to form nitryl chloride ($ClNO_2$) ((1) and (2)). Both $NO_3^{\cdot}$ and N_2O_5 accumulate overnight and enhance $ClNO_2$ production. Acting as a nighttime reservoir, $ClNO_2$ photolyzes at sunrise to release Cl radicals (3) and recycles NO_2, influencing the early NO_x-O_3 cycle[6,14].

$$NO_3 + NO_2 \leftrightarrow N_2O_5 \quad (1)$$

$$N_2O_5 + Cl^- \rightarrow ClNO_2 + NO_3^- \quad (2)$$

$$ClNO_2 + h\nu \rightarrow Cl\cdot + NO_2 \quad (3)$$

Abundant Cl · radicals initiate VOC oxidation, generating peroxy radicals (RO_2 ·), surface O_3, and SOA ((4)–(9)). This nocturnal chlorine chemistry is particularly important in polluted regions[15–17].

$$Cl\cdot + RH \rightarrow HCl + R\cdot \quad (4)$$

$$R\cdot + O_2 \rightarrow RO_2\cdot \quad (5)$$

$$RO_2\cdot + NO \rightarrow RO\cdot + NO_2 \quad (6)$$

[1]Centre for Atmospheric and Climate Sciences, Indian Institute of Technology Madras, Chennai, India. [2]Environmental Engineering Division, Department of Civil Engineering, Indian Institute of Technology Madras, Chennai, India. [3]School of Earth and Atmospheric Sciences, Georgia Institute of Technology, Atlanta, GA, USA. [4]Atmospheric, Oceanic and Planetary Physics, University of Oxford, Oxford, UK. [5]Max Planck Institute for Chemistry, Mainz, Germany. [6]Scripps Institution of Oceanography, University of California, San Diego, La Jolla, CA, USA. [7]Department of Earth and Planetary Sciences, Harvard University, Cambridge, MA, USA. [8]John A. Paulson School of Engineering and Applied Sciences, Harvard University, Cambridge, MA, USA. ✉e-mail: ankitpatel0698@cacs.iitm.ac.in; s.gunthe@iitm.ac.in

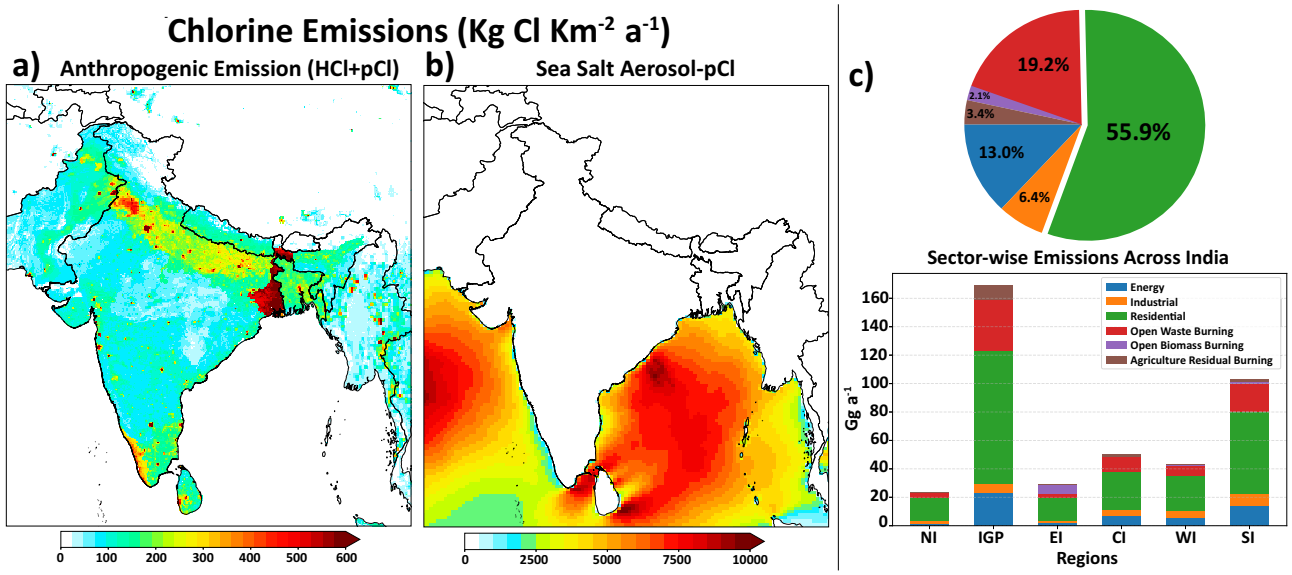

Fig. 1 | Spatial distribution and sectoral contributions of anthropogenic chlorine emissions and sea-salt aerosol chloride flux over India. a Annual anthropogenic chlorine emissions from GT-Chlorine Emission inventory and (**b**) pCl^- emission flux from offline sea-salt aerosol extension in GEOS-Chem[71]. **c** Anthropogenic chlorine emissions ($HCl + pCl^-$) are used from[21] which includes contributions from agricultural residual burning, residential, energy, industry, and open waste burning, open biomass burning. Note the difference in scales between (**a**), (**b**). Pie charts and stacked bar plots represent the percentage (%) and absolute (Gg a^{-1}) contribution of each sector over each region (Fig. S1) of India. Sub-sectoral percentage distribution of HCl and pCl^- is shown in Fig. S2.

$$NO_2 + h\nu \rightarrow NO + O \quad (7)$$

$$O + O_2 \rightarrow O_3 \quad (8)$$

$$RO\cdot + O_2 \rightarrow \text{Carbonyls} + \text{Peroxides} + \text{SOA} \quad (9)$$

India is a global hotspot for chlorine emissions, including high concentrations of gaseous hydrochloric acid (HCl) and particulate chloride (pCl^-)[18,19]. An assessment of chlorine emissions and their impact on Indian air pollution, however, remains limited. Sources include indoor biofuel combustion, waste incineration, industrial processes, crop residue and biomass burning, coal combustion, municipal solid waste, and brick kilns[1,20–22]. Chloride concentrations in Delhi and across the Indo-Gangetic Plain (IGP) frequently exceed those observed in other major global cities, particularly during winter and post-monsoon seasons[1,18,22]. Unlike Europe and North America, where continental chloride largely originates from marine sources via long-range transport, India's atmospheric chloride is predominantly derived from inland anthropogenic HCl and pCl^- emissions[20,21,23,24]. HCl emissions over India range from 40-220 Gg a^{-1} due to waste burning, having a mean of approximately 120 Gg a^{-1}[25] whereas pCl^- is estimated to be 250 Gg a^{-1}, primarily from biomass (~ 68%) and waste burning (~ 21%)[20]. In comparison, China's anthropogenic HCl and pCl^- emissions were 458 and 486 Gg a^{-1}, respectively, in 2014[26], increasing to 756 Gg a^{-1} in 2018[27]. Combined HCl and pCl^- emissions from India are the second-largest after China (~ 913 Gg a^{-1})[21]. For comparison, the United States emitted less than 100 Gg in 2014[28]. Furthermore, India has high ammonia (NH_3) rich atmosphere due to animal husbandry[29,30], creating favorable conditions of rapid particulate ammonium chloride (NH_4Cl) formation through HCl. This process enhances $PM_{2.5}$ pollution and contributes substantially to urban haze and secondary aerosol growth, sometimes accounting for 40-50% of aerosol liquid water content[19,31]. Even so, chlorine chemistry remains poorly investigated as a component of India's air pollution problem.

The objective of this study is to evaluate the impact of anthropogenic chlorine emissions on regional air pollution over India. To achieve this, we have used GEOS-Chem Chemical Transport Model in a high-resolution (0.25° × 0.3125°, ~ 25 km) configuration with hourly outputs for the full year of 2018. The details about the incorporated HCl and pCl^- emission inventory in model (Fig. 1, Figs. S1–S2), detailed model setup and modeled pCl^- validation (Fig. 2) are outlined in methods section. The analysis examines the role of chlorine emissions in regulating the concentrations of pCl^-, $PM_{2.5}$, maximum daily 8-hour average of ozone (MDA8 O_3), and $ClNO_2$. The presented findings show that anthropogenic chlorine emissions and multiphase chlorine chemistry have important roles in modulating regional air quality, particularly over densely populated and industrialized areas. From these results, the recommendation is to incorporate chlorine chemistry and region-specific emission inventories into air quality models of India to better assess the impact of pollution on climate and human health.

Results

Model simulated HCl and pCl^- over India

The spatial distribution of annual average HCl and particulate chloride (pCl^-) concentrations, along with their relative changes between the sensitivity simulations of GEOS-Chem model, one including (Wi-AnthroHCl) and the other excluding anthropogenic HCl + pCl^- emissions (Wo-AnthroHCl), reveals strong spatial heterogeneity across India (Fig. 3). The Indo-Gangetic Plain (IGP) emerges as the most prominent hotspot of HCl, followed by parts of western and southern India, as well as several other urban and industrial clusters (Fig. 3a). High HCl concentrations are largely associated with densely populated regions and intensive anthropogenic activities. In contrast, the spatial pattern of pCl^- (Fig. 3d) shows weaker correspondence with that of HCl, although elevated levels persist over the IGP. Unlike HCl, pCl^- does not exhibit the distinct hotspots observed over western and central India.

In the absence of anthropogenic chlorine emissions, as represented by the Wo-AnthroHCl simulation (Fig. 3b, e), both HCl and pCl^- concentrations become negligible over inland continental regions, with minor residual levels near coastal zones. These concentrations primarily result from marine influences, where HCl is formed through acid displacement reactions or dechlorination of sea-salt aerosols and ocean spray[11,32]. Depending on the seasons, the resulting HCl is transported inland, contributing to small but detectable levels of pCl^- near coastal regions. Figure 3c and f, together with the relative changes shown in Fig. S3, highlight the substantial enhancement of both HCl and pCl^- due to anthropogenic emissions, particularly over the IGP. The sea-salt-derived contribution,

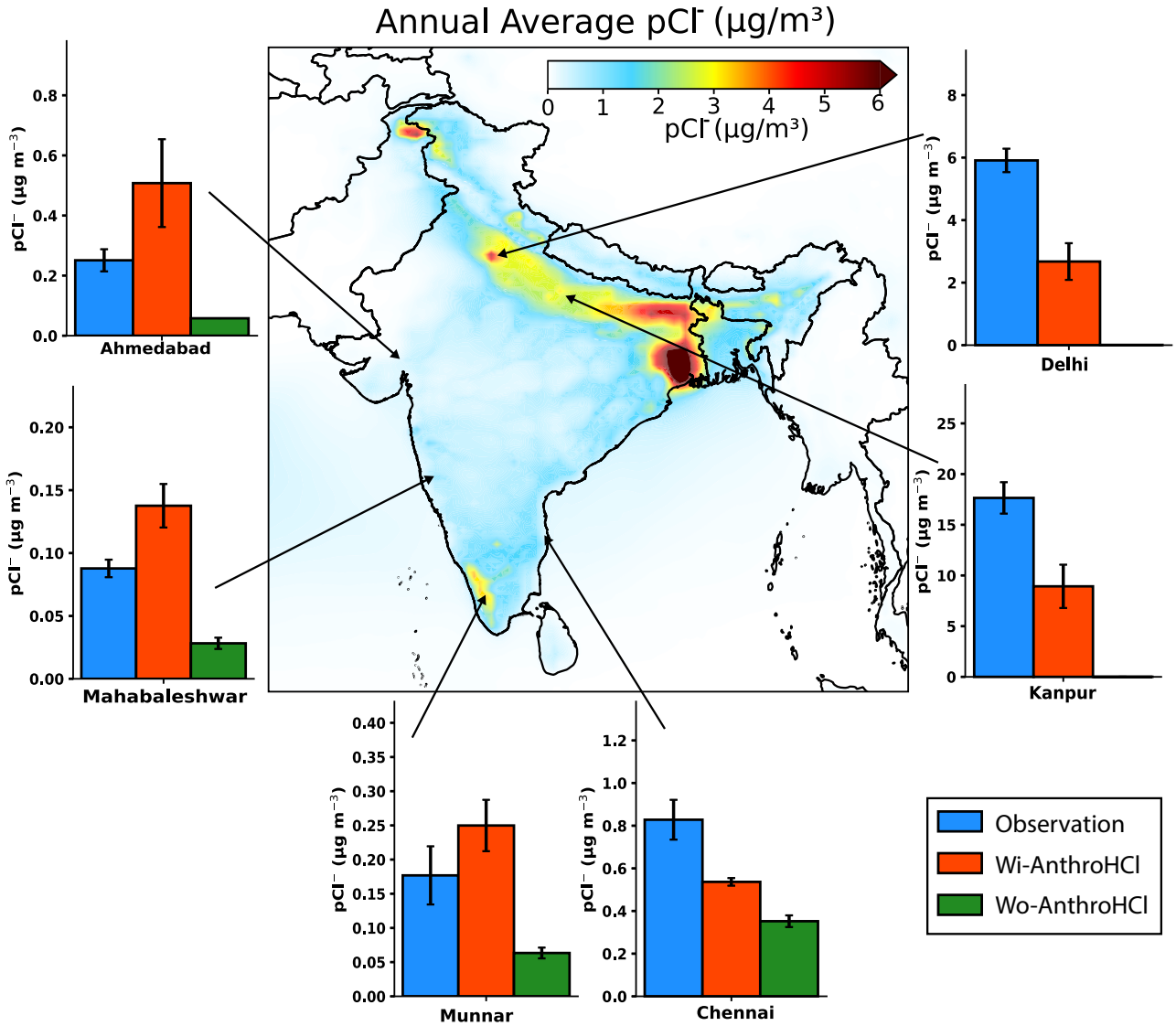

Fig. 2 | Annually averaged modeled pCl^- distribution over India and its validation with different observation datasets. Spatial distribution of annual average particulate chloride (pCl^-, $\mu g\ m^{-3}$) over the Indian region. Bar plots show the comparison between observed and model-simulated (Wi-AnthroHCl and Wo-AnthroHCl) pCl^- concentrations at six monitoring stations, indicated by black arrows on the map. Delhi and Kanpur do not show a Wo-AnthroHCl bar because they are deeply inland sites, with no contribution from marine transport in the Wo-AnthroHCl simulation. These six sites, representing distinct regional markers, were used to validate the modeled pCl^-. Campaign-averaged observations are compared against the corresponding modeled pCl^- concentrations for the same periods.

though evident, remains limited to the southern coastal regions of India, consistent with the spatial patterns shown in Fig. 1b and Fig. S4.

The Indo-Gangetic Plain (IGP) exhibits the highest concentrations of particulate chloride (pCl^-), particularly over Delhi and West Bengal, where distinct hotspots are evident (Fig. 3d). The enhancement in pCl^- arises from gas-to-particle partitioning of HCl in the model, which is highly sensitive to anthropogenic HCl emissions[33]. Seasonal variations Fig. (S5) indicate that pCl^- concentrations are considerably higher in winter and autumn than in summer and spring, reaching a maximum seasonal average of 5.1 $\mu g\ m^{-3}$ during winter. Seasonal anthropogenic chlorine emissions (Fig. S6) reveal relatively weak variability in total emissions across this region, with only modest sector-specific variations. These emission differences are small in magnitude and do not explain the strong seasonal cycle observed in pCl^-. Instead, the pronounced wintertime enhancement of pCl^- primarily reflects the combined effects of lower temperatures, higher relative humidity (RH), and greater aerosol liquid water availability, which shift the HCl partitioning equilibrium toward the particle phase, enhancing the conversion of gaseous HCl to pCl^-[34,35]. Additionally, cooler winter and autumn conditions suppress the reverse conversion of pCl^- to HCl, a process that becomes more efficient at the elevated temperatures typical of spring and summer[12].

The elevated pCl^- levels over the IGP can also be attributed to high chlorine emissions and ammonia-rich environments (Fig. S7), in which HCl readily dissolves into aerosol liquid water. This thermodynamically favors gas-to-particle partitioning through ammonium ($NH4^+$) and pCl^- formation[1,19,36]. In contrast, regions such as Punjab, Jammu & Kashmir, and the western coastal states of Gujarat and Maharashtra exhibit relatively high HCl concentrations (Fig. 3a) yet do not show correspondingly elevated pCl^- levels (Fig. 3d). This is likely attributable to reduced partitioning efficiency, with $pCl^-/(HCl+pCl^-)$ ratios below 0.4 (40%) and RH values ≤50% (Fig. S8). Under such drier conditions, limited aerosol liquid water content (ALWC) restricts the aqueous dissolution and ionization processes that drive $NH4^+$ and pCl^- formation[1,31,36].

Interestingly, despite relatively lower HCl and NH_3 concentrations, the southwestern coastal regions, particularly Kerala and coastal Karnataka, exhibit notably high pCl^- abundance. This area also shows a significantly elevated $pCl^-/(HCl+pCl^-)$ ratio (Fig. S8), indicating efficient partitioning

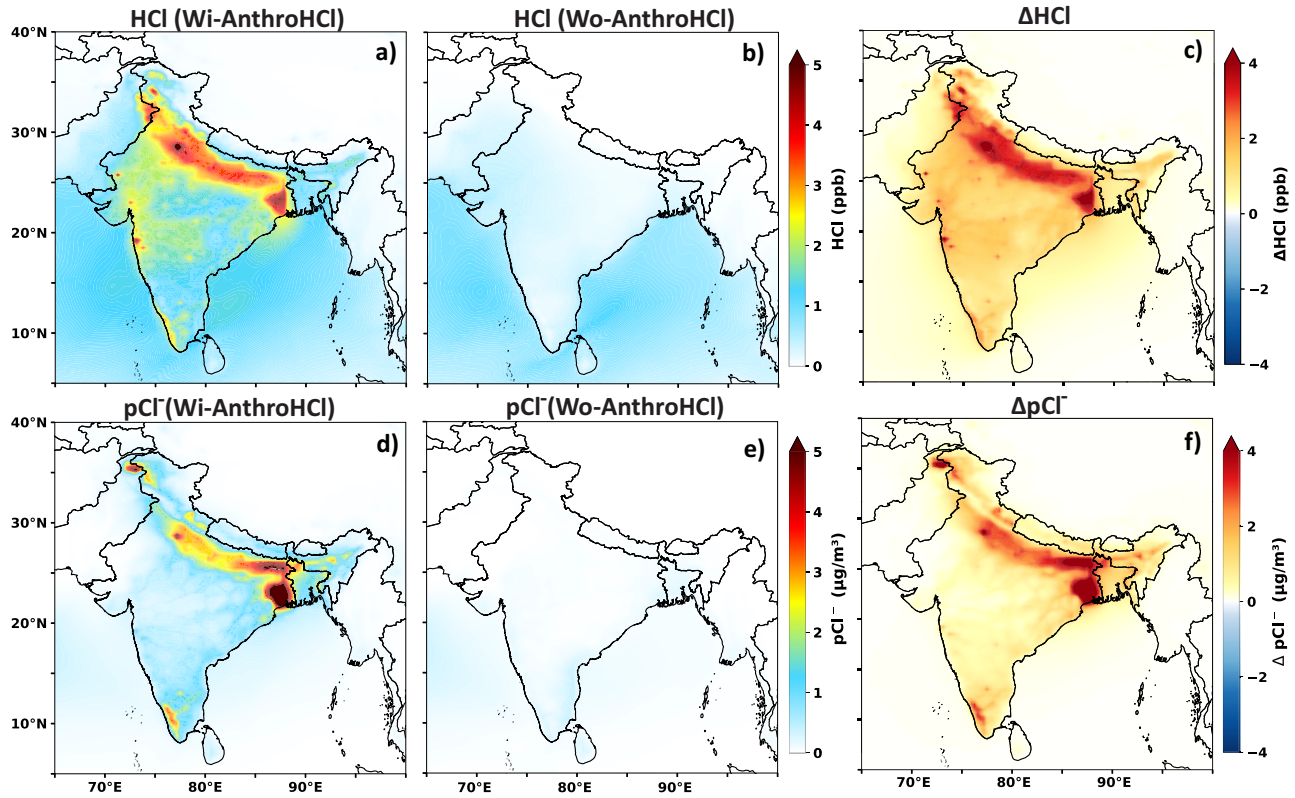

Fig. 3 | Annual mean HCl and pCl^- and their absolute relative differences between Wi-AnthroHCl and Wo-AnthroHCl simulations. Spatial distribution of annually averaged HCl (**a**, **b**) and pCl^- (**d**, **e**) concentrations from Wi-AnthroHCl and Wo-AnthroHCl model simulations. **c**, **f** represent the annual averaged absolute difference for both HCl and pCl^- when taking the difference of Wi-AnthroHCl and Wo-AnthroHCl model simulations for year the 2018.

into the particulate phase. In addition to moderate chlorine emissions relative to adjacent regions (Fig. 1), persistently high RH (70–80% throughout most of the year) strongly promotes such a chemical regime and behavior. Under such humid conditions, chloride partitioning increases sharply from approximately 0.4 at RH ≤50% to about 0.95 at RH ≥50%, enabling even low HCl concentrations to efficiently transition to the particle phase[36]. Moreover, the marine boundary layer in these regions contains substantial sea-salt aerosol contributions that supply additional chloride sources[37,38]. Elevated ALWC under coastal humid conditions enhances heterogeneous chemistry and aerosol growth[31,39]. This mechanism contrasts with the ammonia-driven partitioning prevalent in the IGP, demonstrating that high humidity and marine influences can sustain significant pCl^- formation even in environments with limited NH_3 availability[19,37].

Chlorine emission-driven perturbations in key pollutants

Enhancement of $ClNO_2$ via chlorine emissions. The spatial distribution of annually-averaged nighttime maximum $ClNO_2$ concentrations highlights the strong influence of anthropogenic chlorine emissions on nighttime chemistry across India (Fig. 4). Here, 'nighttime maximum' refers to the highest $ClNO_2$ values obtained within the 21:00–09:00 local time window, which represents the period of $ClNO_2$ accumulation during the night and early morning before rapid photolysis after sunrise. The inclusion of anthropogenic HCl emissions in the Wi-AnthroHCl simulation results in an annual mean nighttime $ClNO_2$ enhancement exceeding 700 ppt over high-emission continental regions, whereas the eastern coastal areas remain dominated by marine chlorine sources even in the absence of anthropogenic chlorine inputs (Fig. 4b).

The primary nighttime formation pathway for $ClNO_2$ involves the heterogeneous uptake of N_2O_5 on chloride-containing aerosols under NO_x-rich conditions (Reactions (2) and (3)), which converts otherwise inert particulate chloride into highly reactive $ClNO_2$, establishing an important nocturnal reservoir of chlorine. Its subsequent photolysis increases chlorine radicals (Cl ·) in the morning hours, which enhances the oxidation of VOCs and carbon monoxide (CO), producing peroxy radicals (RO_2 and HO_2) that accelerate photochemical ozone production[6,40]. Consistent with this mechanism, our global sensitivity simulations indicate that the inclusion of anthropogenic HCl emissions leads to an annual mean enhancement in OH of up to ~ 8% in some regions, as reported by previous studies[11].

The highest concentrations and the largest spatial extent of $ClNO_2$ are observed in winter and autumn, whereas lower levels are found in the spring and summer seasons (Fig. S9). Elevated $ClNO_2$ concentrations during winter and autumn are primarily associated with higher levels of particulate chloride (pCl^-) and N_2O_5 during these seasons. The aqueous-phase chloride concentration plays a crucial role in determining $ClNO_2$ yield[41]. Additionally, the eastern coastal regions consistently exhibit higher $ClNO_2$ concentrations than the western coast, underscoring the enhanced influence of chlorine chemistry along the coastal Bay of Bengal. The most significant positive changes are concentrated over the Indo-Gangetic Plain (IGP), coinciding with regions of high anthropogenic chlorine emissions.

By contrast, summer exhibits the lowest $ClNO_2$ concentrations, primarily due to reduced availability of N_2O_5 and pCl^-. These reductions occur because of unfavorable conditions for N_2O_5 formation during this season[42], as rapid photolysis of the NO_3 radical under extended daylight hours and elevated temperatures shifts the NO_3-N_2O_5 equilibrium toward NO_3^-. Overall, the simulations reveal substantial enhancements in $ClNO_2$ across much of the Indian subcontinent, highlighting the potentially significant role of anthropogenic chlorine emissions in modifying nocturnal oxidation chemistry. However, the lack of observational data in these regions underscores the urgent need for targeted field measurements to validate model predictions, reduce current uncertainties[8], and better quantify the impacts of chlorine species on regional atmospheric composition.

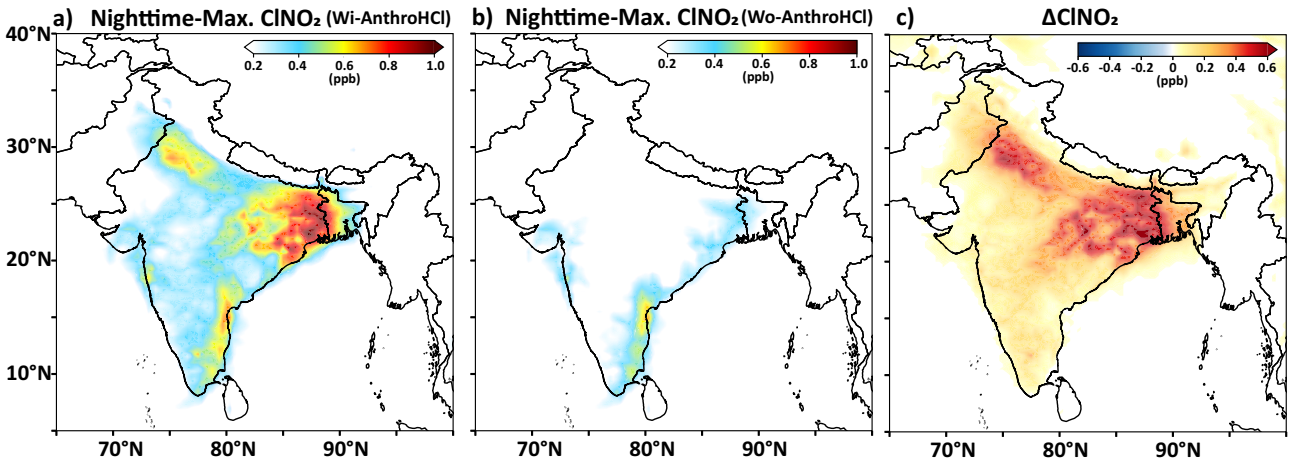

Fig. 4 | Anthropogenic influence on nighttime $ClNO_2$ concentrations over India. Spatial distribution of annually averaged nighttime $ClNO_2$ concentrations from GEOS-Chem simulations using an accumulation window from 21:00 to 09:00 local time. **a** shows the Wi-AnthroHCl simulation, highlighting the contribution of anthropogenic sources. **b** presents the Wo-AnthroHCl simulation, representing the background levels of $ClNO_2$ driven mainly by natural or marine-influenced sources. **c** illustrates the difference ($\Delta ClNO_2$) between Wi-AnthroHCl and Wo-AnthroHCl (**a**–**b**), isolating the net effect of anthropogenic HCl emissions on nighttime $ClNO_2$. This comparison clearly reveals the regions where anthropogenic chlorine plays a dominant role in modulating nocturnal chemistry.

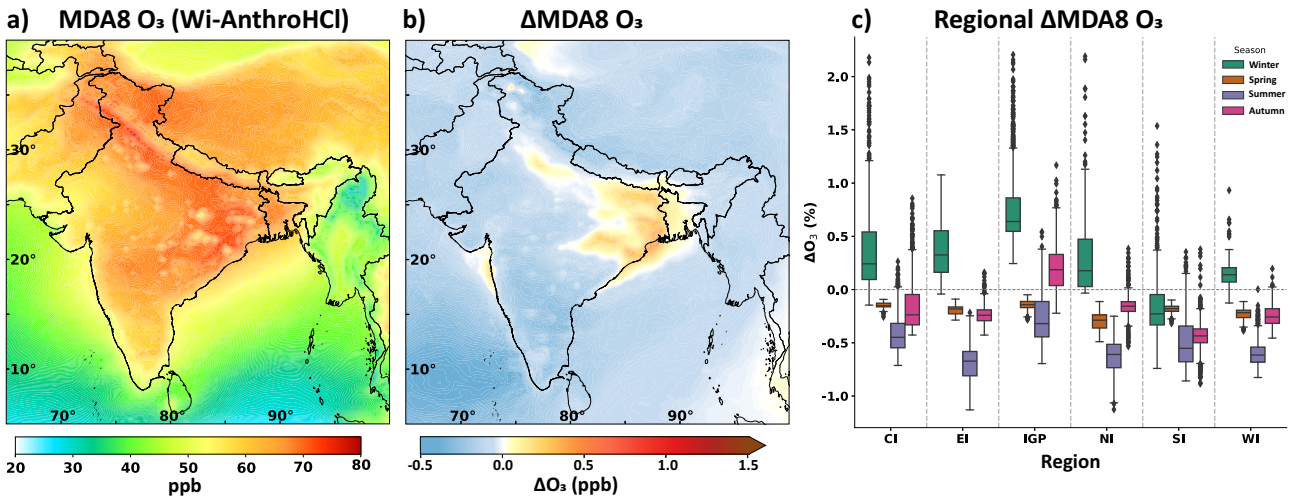

Fig. 5 | Annual and seasonal impacts on MDA8 O_3 across India. Spatial distribution of annually averaged (**a**) MDA8 O_3 of model simulation having anthropogenic HCl emissions and (**b**) changes in ΔMDA8 O_3 by taking the difference of Wi-AnthroHCl and Wo-AnthroHCl simulations, (**c**) Seasonal distribution of ΔMDA8 O_3 across Indian regions. Each box represents the interquartile range (IQR) with the median line, whiskers extending to 1.5 × IQR. Seasonal variations are shown for all four seasons for each region of India as divided in Fig. S1.

Influence on surface ozone variability. The impact of anthropogenic chlorine emissions is reflected in the spatial patterns and seasonal variations of changes in maximum daily 8-hour average ozone (ΔMDA8 O_3) across India. Figure 5 presents (a) the annually averaged MDA8 O_3 in Wi-AnthroHCl simulation, (b) its absolute changes (ΔMDA8 O_3) between the Wi-AnthroHCl and Wo-AnthroHCl simulations, and (c) the corresponding regional and seasonal relative changes. MDA8 O_3 exhibits pronounced spatial heterogeneity and strong seasonal variability across the Indian subcontinent, with lower concentrations during autumn and winter and higher levels during spring and summer. This pattern reflects the strong dependence of ozone formation on solar radiation, as also shown by the absolute seasonal changes in Fig. S10.

Previous studies over China have reported annual mean ozone increases of 1.9 ppb (3.2%), 2.5 ppb (5.3%), and 2.0 ppb (4.1%) in response to anthropogenic chlorine emissions[11,33,43]. Over Europe, monthly mean ozone increases by 0.22 and 0.41 (1.2%) ppb in summer, with a 0.2–1.6 ppb increase over the Northern Hemisphere[24,44,45], while in the United States, a 1–2 ppb increase is observed (in February and September), with even smaller changes (< 0.3 ppb, July) over New York[46,47]. However, the reported studies over Europe and the United States exclude detailed anthropogenic chlorine sources, and these impacts are mostly dominated by long-range transport of SSA[23,24]. Moreover, these studies primarily focus on the overall effects of chlorine-halogen chemistry, rather than explicitly isolating the contribution from anthropogenic chlorine emissions. Consequently, these ozone responses over Europe and the United States cannot be directly compared with the ozone responses to anthropogenic chlorine emissions, as investigated in the present study.

Our simulations reveal both positive and negative changes in ΔMDA8 O_3, with substantial spatial and seasonal variability. Although the overall magnitude of the annual mean change remains modest in our analysis, distinct regional and seasonal features clearly emerge. The largest increases in ΔMDA8 O_3 occur over the Indo-Gangetic Plain (IGP) during winter and

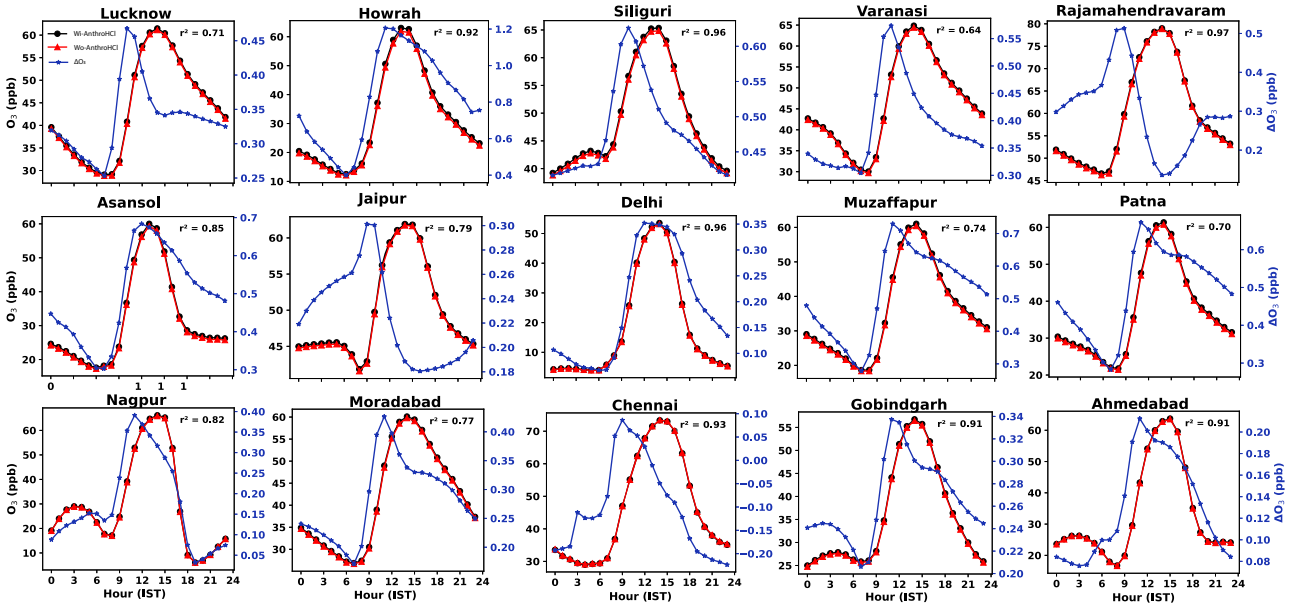

Fig. 6 | Impact on wintertime diurnal variation in ozone. Averaged diurnal variations in O_3 and ΔO_3 during the winter season from Wi-AnthroHCl and Wo-AnthroHCl simulations where ΔO_3 is calculated as a difference between Wi-AnthroHCl and Wo-AnthroHCl simulations. The r^2 represents the coefficient of determination when the modeled O_3 is compared with surface observation of O_3 provided by CPCB at each station.

autumn, which is consistent with the seasonal behavior reported for the Yangtze River Delta Region in China[12]. These increases are mainly driven by enhanced biomass and residential burning emissions of chlorine and the longer nighttime durations prevalent in high-emission regions[11] combined with lower boundary layer mixing heights[48]. In contrast, southern India (SI) shows no significant positive change in any season. Spatially, the positive ozone changes correspond well with regions exhibiting higher ΔHCl and ΔpCl^- values (Fig. 3), suggesting that elevated anthropogenic chlorine emissions enhance ozone formation; however, the change remains minimal. The seasonally averaged ΔMDA8 O_3 across India is estimated to be −0.19% (−0.14 ppb) in spring, −0.47% (−0.23 ppb) in summer, −0.15% (−0.09 ppb) in autumn, and +0.28% (+0.17 ppb) in winter. The IGP shows the highest relative increases among all regions, with a maximum of +0.76% (+0.44 ppb) during winter (Fig. 5c).

Notably, regions with positive $\Delta ClNO_2$ (Fig. 4c) exhibit concurrent increases in ΔMDA8 O3 (Fig. 5b), suggesting a strong spatial correlation between chlorine activation and ozone enhancement. Conversely, during summer, most regions including the IGP, exhibit negative ΔMDA8 O_3 values, indicating that chlorine chemistry suppresses surface ozone. Similar behavior has been noted in previous studies[12,43], where chlorine reactions were found to reduce ozone during the warm season. The reduced effectiveness of $ClNO_2$ chemistry in summer arises from higher temperatures, shorter nights, and lower nighttime N_2O_5 levels, potentially making the $ClNO_2$ pathway less significant[23]. Furthermore, under intense solar radiation, $ClNO_2$ photolysis fails to efficiently recycle NO to NO_2, instead enhancing NO_x scavenging (via $NO_2 + OH \rightarrow HNO_3$) and ozone titration, thereby lowering ozone production efficiency. Increased HO_2 and Cl radical reactions also contribute to catalytic ozone loss by reacting with O_3 to form HOCl, which photolyzes rapidly, leading to further ozone depletion[13,23].

The effect of anthropogenic chlorine emissions on the diurnal cycle of surface ozone is illustrated in Fig. 6, which presents the averaged diurnal variations of O_3 from Wi-AnthroHCl and Wo-AnthroHCl simulations, along with their differences (ΔO_3) mapped over Central Pollution Control Board (CPCB) monitoring stations across India. The coefficients of determination (r^2) between modeled and observed O_3 are included for each diurnal cycle. Winter is the only season showing positive ΔO_3, with the strongest enhancement over the IGP. The ΔO_3 patterns indicate that anthropogenic chlorine emissions significantly increase morning-time O_3 concentrations (09:00-11:00 local time), corresponding to the photolysis of nighttime-accumulated $ClNO_2$ and subsequent release of Cl radicals. These radicals accelerate VOC oxidation, leading to early morning ozone peaks (reactions (5)-(9)). Consequently, under strong chlorine emission episodes, the daily ozone maximum may shift toward earlier hours, or an additional morning ozone peak may emerge alongside the typical afternoon maximum. Such temporal shifts in O_3 peaks could have adverse health implications and alter the photochemistry of the environment during winter mornings over densely populated regions.

Overall, our results indicate that the magnitude of tropospheric ΔO_3 over India is smaller that reported for China, reflecting a weaker sensitivity to anthropogenic chlorine emissions (Fig. S11), where ozone exhibits a substantially stronger response to chlorine perturbations. This contrast suggests that India and China may operate under distinct chemical regimes of ozone formation with respect to chlorine chemistry. Such a complex and nonlinear spatiotemporal response of ozone to HCl emissions requires further investigations using chemical box models and will be covered in follow-up studies. This will help to elucidate as to why, despite the IGP being one of the most polluted places across the globe, it exhibits relatively lower average ozone responses to chlorine emissions as compared to similar polluted sites in China[11]. Therefore, further high-resolution modeling and observational studies are needed to elucidate the underlying chemical mechanisms governing these regional differences.

Impact on $PM_{2.5}$ and its components. The influence of anthropogenic chlorine emissions on fine particulate matter over India is evident from the annually averaged differences in $PM_{2.5}$ concentrations between the Wi-AnthroHCl and Wo-AnthroHCl simulations (Fig. 7). The spatial distribution of $\Delta PM_{2.5}$, along with the box plots representing respective changes in each region across India (regional divisions shown in Fig. S1), illustrates consistent increases in $PM_{2.5}$ concentrations following the inclusion of chlorine emissions in all four seasons. The most affected regions include the Indo-Gangetic Plain (IGP), parts of northern India (NI), and Kerala in southern India (SI).

Seasonal variations in $\Delta PM_{2.5}$ (Fig. S12) reveal that the largest increases in $PM_{2.5}$ occur during winter (+ 2.09 $\mu g\,m^{-3}$, +2.71%), followed by autumn (+ 1.96 $\mu g\,m^{-3}$, +2.67%). Spring exhibits the lowest enhancement (+ 0.07 $\mu g\,m^{-3}$, +0.28%), primarily affecting northern India. The annual

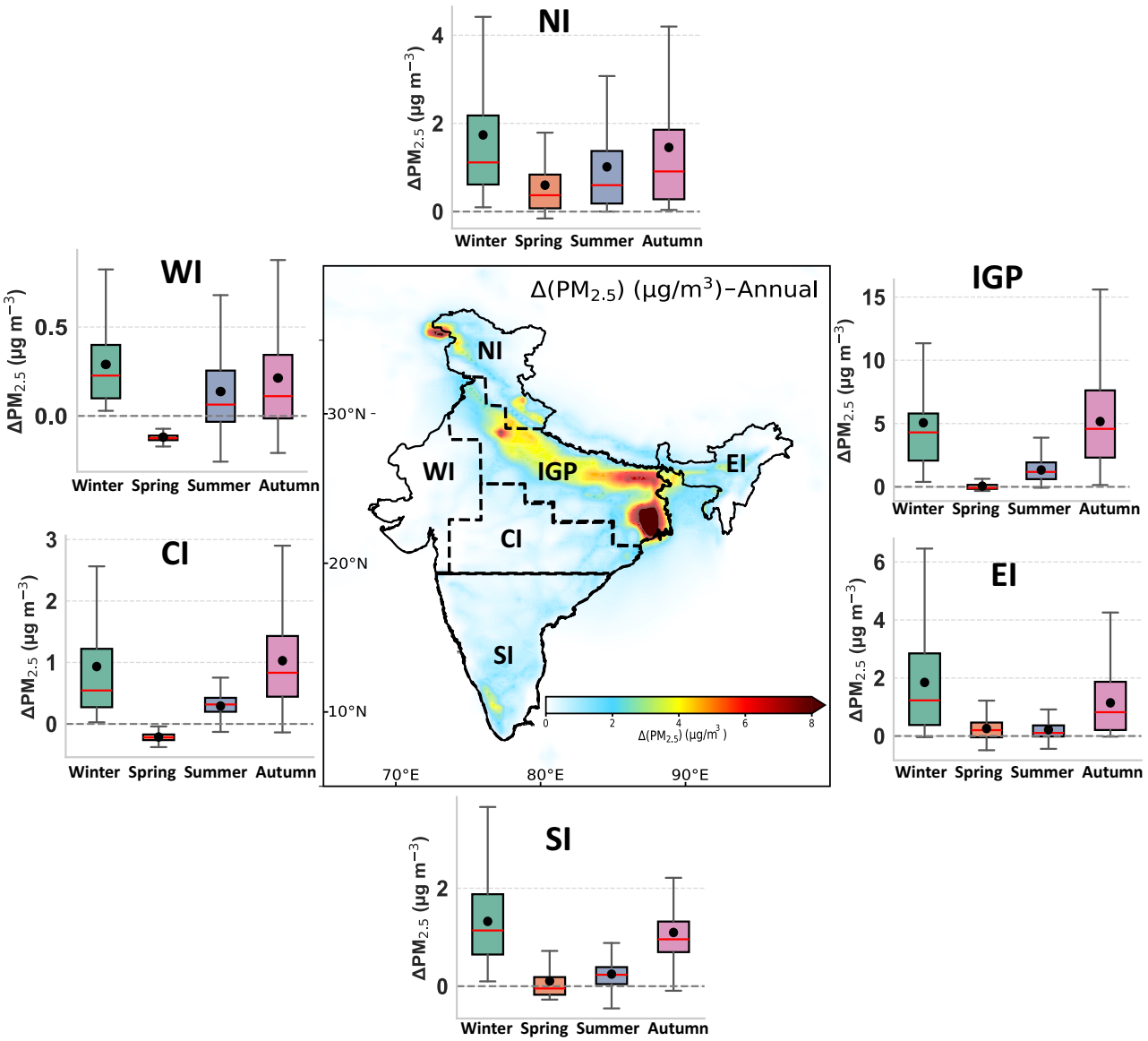

Fig. 7 | Regional and seasonal sensitivity of $\Delta PM_{2.5}$ to anthropogenic chlorine emissions across India. Spatial distribution of annual averaged $\Delta PM_{2.5}$ and seasonal variability in the sensitivity of $\Delta PM_{2.5}$ concentrations to chlorine emissions. Box plots show the regional changes in $\Delta PM_{2.5}$ ($\mu g\ m^{-3}$) derived from the difference between Wi-AnthroHCl and Wo-AnthroHCl simulations. Each box represents the $\Delta PM_{2.5}$ within a specific region for each season, highlighting both the magnitude and spread of the response to anthropogenic chlorine emissions. Note the difference in scales across box plot panels to better capture the variability in regions with smaller $\Delta PM_{2.5}$, as using a uniform scale would mask these variations.

mean $PM_{2.5}$ rises by + 1.18 $\mu g\ m^{-3}$ (+1.64 %) nationally, with the greatest increase over IGP (+ 2.9 $\mu g\ m^{-3}$, +2.6%), particularly around New Delhi and West Bengal, followed by NI (+ 1.2 $\mu g\ m^{-3}$, +4%). Although these values may appear modest when averaged annually, the box plots in Fig. 7 indicate strong seasonal variability. During winter, the enhancement reaches + 5.1 $\mu g\ m^{-3}$ (+4%) over the IGP and + 1.75 $\mu g\ m^{-3}$ (+7.3%) over NI. The spatial distribution of annual relative changes is further presented in Fig. S13.

To better understand the composition driving these increases, Fig. 8 shows the spatial distribution of annually averaged changes in individual $PM_{2.5}$ components (pCl^-, $NH4^+$, $SO_4{}^{2-}$, NO_3^-) derived from the difference between the Wi-AnthroHCl and Wo-AnthroHCl simulations. The results indicate that pCl^- and NH_4^+ are the primary contributors to the overall $PM_{2.5}$ enhancement, with annual average increases of + 0.91 $\mu g\ m^{-3}$ and + 0.41 $\mu g\ m^{-3}$, respectively, across the Indian region. These species also exhibit notable seasonal dependence (Figs. S14–S16).

Enhancement in NH_4^+ concentrations over the region is due to reactions of excess NH_3[29] with HCl. Conversely, nitrate (NO_3^-) concentrations decrease in all seasons except summer (Fig. S14), primarily due to the suppression of N_2O_5 hydrolysis (reaction 1, in supplement) by elevated pCl^- levels. Instead of hydrolysis, N_2O_5 reacts with chloride to form $ClNO_2$ (reaction 2, in supplement), thereby reducing the overall efficiency of nocturnal nitrate formation[49–51]. During summer, however, ΔNO_3^- becomes positive (Fig. S15) because $ClNO_2$ chemistry is less active, allowing nitrate to form via heterogeneous N_2O_5 uptake[52].

In contrast, sulfate (SO_4^{2-}) concentrations show relatively greater changes than nitrate, with a decrease observed across most regions of India (Fig. 5, Fig. S16). This reduction in SO_4^{2-} arises from the competition between HCl and H_2SO_4 for ammonia in aerosol thermodynamic system, whereby the presence of HCl drives ammonia preferentially towards NH_4Cl formation[19] (reaction 3-4, in supplement). Consequently, less NH_{4+} is available for sulfate neutralization, leading to lower SO_4^{2-} concentrations.

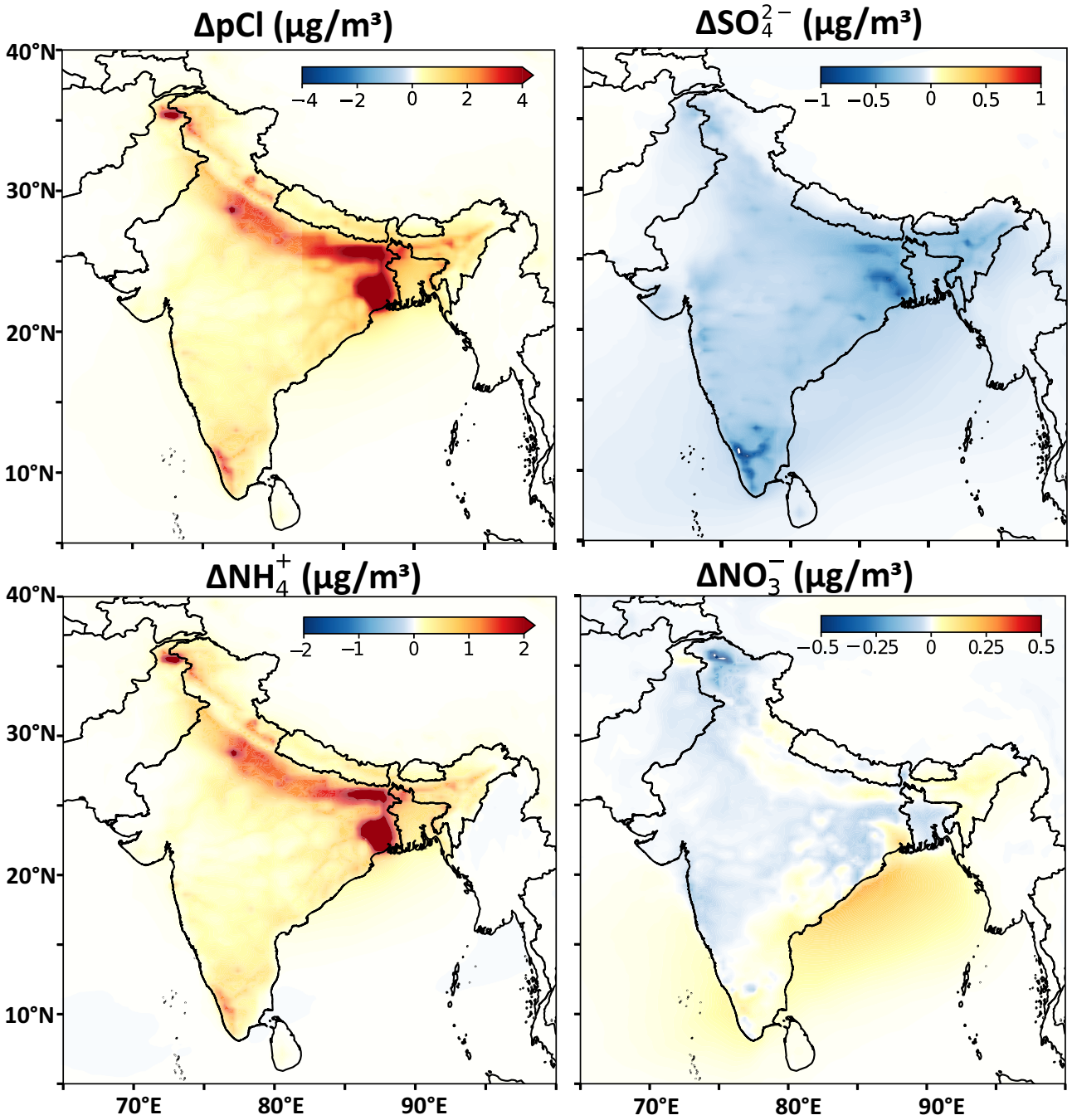

Fig. 8 | Impact of anthropogenic chlorine emissions on the chemical components of $PM_{2.5}$. Annual changes in the chemical components of $PM_{2.5}$ arising from the influence of anthropogenic chlorine emissions. The panels present the differences (Δ) between Wi-AnthroHCl and Wo-AnthroHCl simulations for particulate chloride (pCl^-), sulfate (SO_4^{2-}), ammonium (NH_{4+}), and nitrate (NO_3^-).

Discussion

This study provides a comprehensive assessment of anthropogenic chlorine emissions and their impacts on regional air chemistry over India, demonstrating that chlorine is a key, non-linear, and previously underrepresented driver of regional air quality. Over the IGP, home to ~ 700 million people, anthropogenic chlorine increases wintertime $PM_{2.5}$ by up to + 5.1 $\mu g\ m^{-3}$ (+4%), aggravating exposure to fine particulates associated with respiratory and cardiovascular diseases and premature mortality[53,54]. Chlorine-rich aerosols also contribute to visibility degradation by enhancing aerosol water uptake and hygroscopic growth. Future studies should examine the effects of chlorine-containing particles on aerosol optical properties and their role in wintertime haze formation over the region.

The comparatively weaker and non-linear ozone response to chlorine emissions compared to China indicates distinct chemical regimes across India and the need for high-resolution regional and box-model studies to elucidate chlorine-driven ozone production and loss. This also implies that findings from East Asian studies cannot be directly applied to South Asia, underscoring the importance of region-specific assessments. Enhanced nighttime formation of $ClNO_2$ shifts peak ozone to early morning hours, coinciding with commuting periods and shallow boundary layers, potentially increasing human exposure.

Current emission inventories strongly underestimate inland chlorine sources and poorly constrained emissions such as Cl_2, HOCl, chlorinated VOCs, plastic burning, brick kilns, and steel pickling create large uncertainties in chlorine budgets. Given strong spatial heterogeneity and chemical regimes, region-specific inventories and improved representation of primary and multiphase secondary chlorine-VOC chemistry are urgently required to better assess oxidation capacity and secondary organic aerosol formation.

Future efforts must explicitly address chlorine emission control. Reducing NH_3 emissions to limit pCl^- production is unrealistic in agriculturally dominated regions; direct control of primary HCl sources is therefore more feasible. Effective mitigation requires stricter enforcement against open burning, improved waste management, and regulation of industrial emissions. Experience from China shows that cleaner fuels, stronger industrial standards, and the adoption of HCl scrubbers and flue-gas desulfurization systems (> 95% removal efficiency) can substantially reduce reactive chlorine emissions. Future studies should prioritize quantifying HCl emissions from informal sectors, waste management, and plastic burning to support mitigation strategies.

Looking ahead, targeted observations of HCl, pCl^-, Cl_2, N_2O_5, and $ClNO_2$ using chemical ionization mass spectrometry (CIMS) and high-resolution aerosol mass spectrometry (AMS) across inland, coastal and urban regions, especially in winter, are critically important to constrain nocturnal processes, morning photochemical transitions and model uncertainties.

Methods

GEOS-chem model setup

We used the GEOS-Chem chemical transport model (v14.4.2; https://zenodo.org/records/12807579) which contains a detailed NO_x-Ox-VOC-PM-halogen (Br-Cl-I) chemistry[55]. GEOS-Chem was driven by offline assimilated meteorological fields from GEOS-FP (Goddard Earth Observing System- forward processing) having 47 vertical hybrid pressure-sigma levels up to 0.01 hPa with native horizontal resolution of 0.25° × 0.3125° provided by NASA's Global Modeling and Assimilation Office (GMAO). For the given study, we run the GEOS-Chem model both on a global scale and then at a nested domain over India using its standard full chemistry simulation with a simple SOA (secondary organic aerosol) scheme which follows fixed yield approach for SOA formation in the model[56,57]. The dynamical boundary conditions generated every 3 h from a global simulation (2° × 2. 5°) were used to conduct nested-grid simulations (0.25° × 0.3125°, ~ 25km) at every hour over the Indian region (5° S-45° N, 55°-105° E) for one full year of 2018, following 6 month spin-up time. GEOS-Chem has been previously used and showed a reasonable reproducibility of pollutants over Indian region and provides a wide range of research topics in atmospheric chemistry and air quality[58–61].

GEOS-Chem has a detailed chlorine chemistry mechanism developed by refs. 11,16 and heterogeneous reactions of $N_2O_5 - ClNO_2$ mechanism based on ref. 62. Tropospheric halogen chemistry, as simulated in previous studies[16,63], was extended by ref. 11 to include chloride mobilization from sea-salt aerosol (SSA) through HCl acid displacement and other heterogeneous processes. The mechanism treats both fine-mode (< 0.5 μm) and coarse-mode (> 0.5 μm) pCl^- and detailed gas-phase inorganic chlorine species[16,27]. In the default GEOS-Chem configuration, the primary source of tropospheric chlorine is governed by pCl^- release from SSA in fine and coarse modes[11,27]. Chlorine Emissions are added as HCl and ISORROPIA-II repartitions between particle and gas phases are included as part of the $H_2SO_4 - HCl - HNO_3 - NH_3$ – NVCs thermodynamic system[11,34].

Emissions

Emissions in the GEOS-Chem model are implemented through the HEMCO (Harvard-NASA Emissions Component) module, which provides flexible configurations for different emission types[64]. The global anthropogenic emissions of SO_2, NO_x, CO, NMVOC and NH_3 were taken from the Hemispheric Transport of Air Pollution (HTAP_v3-2018) inventory (https://edgar.jrc.ec.europa.eu/dataset_htap_v3). Biogenic emissions of VOC were taken from MEGAN v2.1[65] and Global Fire Emissions Database version 4 (GFED4) was implemented for biomass burning emisisons (ref. 66). Continental inorganic chlorine emissions were taken from a recently developed global HCl emission inventory (GT-Emission Inventory) gridded at a spatial resolution of 0. 1° × 0. 1° by[21]. This inventory provides continental chlorine emissions in the form of HCl and pCl^- for 6 different sectors as mentioned in Fig. 1. India contributes 380 Gg a^{-1} to the total global HCl emissions of 4731 Gg a^{-1} with 213 Gg a^{-1} from the residential sector, 76 Gg a^{-1} from open waste burning, 49 Gg a^{-1} from energy, 25 Gg a^{-1} from industry, 13 Gg a^{-1} from agricultural residue burning, and 8 Gg a^{-1} from open biomass burning. These sectors consider sources of HCl and pCl^- from coal combustion, solid waste and biomass combustion, indoor biofuel, coke and brick production. Sub-sector wise percentage distribution of HCl and pCl^- over the Indian region is shown in Fig. S2, more details can be found in[21]. For this study, we performed two simulations using the GEOS-Chem model, one including anthropogenic HCl + pCl^- emissions (Wi-AnthroHCl) and another excluding anthropogenic HCl + pCl^- emissions (Wo-AnthroHCl).

Observations and model evaluation

We used multiple data sets of observations for the GEOS-Chem performance evaluation. We compared the modeled pCl^- with observations for six different locations in India, each from different campaigns. These locations are Delhi (28.61 °N, 77.23 °E), Chennai (13.08 °N, 80.27 °E), Ahmedabad (23.03 °N, 72.58 °E), Kanpur (26.45 °N, 80.35 °E), Mahabaleshwar (17.92 °N, 73.65 °E) and Munnar (10.09 °N, 77.06 °E). Out of six locations, pCl^- for four are obtained from published sources[1,22,67]; (Table S1). It should be acknowledged that, due to the limited availability of chloride measurements in the Indian region, some of the observational datasets used for comparison are drawn from different years, ignoring the potential uncertainties related to interannual variability. In India, $ClNO_2$ had been measured only in Delhi[68], our model results were evaluated against its published measurements (Fig. S17). We used hourly data of O_3 and $PM_{2.5}$ provided by the Central Pollution Control Board (CPCB, https://airquality.cpcb.gov.in/ccr/#/caaqm-dashboard-all/caaqm-landing/, last access on 20 June 2025). Model-simulated mean surface concentrations from the nearest grid cell are compared with observations (Table S2).

Figure 2 presents a comparison between simulated pCl^- concentrations and observations from six distinct field campaigns across different regions of the Indian subcontinent. The model successfully captures the spatial variability and magnitude ranges of pCl^- at these sites (Table S3), reflecting diverse regional characteristics. However, pCl^- is overestimated at western coastal sites, where strong marine influence already leads to high background chloride levels. The addition of anthropogenic HCl, together with high relative humidity and potential overestimation of sea-salt aerosol emissions in GEOS-Chem under high-wind coastal conditions[69,70], likely enhances chloride retention in the particle phase. In contrast, the model tends to underestimate pCl^- concentrations at high-emission locations like Delhi and Kanpur. This discrepancy may arise because the model configuration does not include emissions from certain chlorine-containing species such as Cl_2, CH_2Cl_2, and $CHCl_3$, which are predominantly emitted from industrial activities dominant in these regions. Additionally, the current model simulation lacks chlorine emissions from other key sources such as plastic burning and steel pickling industries and the GT-Emission inventory reportedly underestimates biomass burning emissions in India by approximately an order of magnitude (~ 10 ×) as documented by ref. 3. To compensate for these underestimations, we applied the scaling factor to anthropogenic HCl emissions, which significantly improved the agreement between the modeled and observed pCl^- concentrations.

Data availability

Data of anthropogenic HCl and pCl emissions with sectoral distribution, GEOS-Chem diagnostics are available at https://doi.org/10.5281/zenodo.19002241. Surface observation of Ozone can be found at https://cpcb.nic.in/.

Due to the extremely large data size, associated storage capabilities and transfer limitations, all datasets generated from GEOS-Chem simulations are not publicly hosted. However, such data can be made available from the corresponding author upon reasonable request.

Code availability

The GEOS-Chem v14.4.2 code used in this study can be accessed from https://zenodo.org/records/12807579. Python-v3.11.7 codes generated for analysis in this study can be found here: https://doi.org/10.6084/m9.figshare.31704745.

Received: 19 December 2025; Accepted: 17 March 2026;
Published online: 02 April 2026

References

1. Gunthe, S. S. et al. Enhanced aerosol particle growth sustained by high continental chlorine emission in India. *Nat. Geosci.* **14**, 77–84 (2021).
2. Ojha, N. et al. On the widespread enhancement in fine particulate matter across the Indo-Gangetic Plain towards winter. *Sci. Rep.* **10**, 5862 (2020).
3. Chang, D. et al. Significant chlorine emissions from biomass burning affect the long-term atmospheric chemistry in Asia. *Natl. Sci. Rev.* **11**, nwae285 (2024).
4. Ravishankara, A. Are chlorine atoms significant tropospheric free radicals? *Proc. Natl. Acad. Sci. USA* **106**, 13639–13640 (2009).
5. Saiz-Lopez, A. & von Glasow, R. Reactive halogen chemistry in the troposphere. *Chem. Soc. Rev.* **41**, 6448–6472 (2012).
6. Thornton, J. A. et al. A large atomic chlorine source inferred from mid-continental reactive nitrogen chemistry. *Nature* **464**, 271–274 (2010).
7. Crisp, T. A. et al. Observations of gas phase hydrochloric acid in the polluted marine boundary layer. *J. Geophys. Res.: Atmos.* **119**, 6897–6915 (2014).
8. Saiz-Lopez, A. et al. The influence of short-lived halogens on atmospheric chemistry and climate. *Nature* **648**, 289–299 (2025).
9. Dhulipala, S. V., Bhandari, S. & Ruiz, L. H. Formation of oxidized organic compounds from Cl-initiated oxidation of toluene. *Atmos. Environ.* **199**, 265–273 (2019).
10. Sommariva, R. et al. Enhanced wintertime oxidation of VOCs via sustained radical sources in the urban atmosphere. *Environ. Pollut.* **274**, 116563 (2021).
11. Wang, X. et al. Effects of anthropogenic chlorine on $PM_{2.5}$ and Ozone air quality in China. *Environ. Sci. Technol.* **54**, 9908–9916 (2020).
12. Yi, X. et al. Significant impact of reactive chlorine on complex air pollution over the Yangtze River Delta region, China. *J. Geophys. Res. Atmos.* **128**, e2023JD038898 (2023).
13. Zhang, Y. et al. Impacts of chlorine emissions on secondary pollutants in China. *Atmos. Environ.* **246**, 118177 (2021).
14. Simpson, W. R., Brown, S. S., Saiz-Lopez, A., Thornton, J. A. & von Glasow, R. Tropospheric halogen chemistry: Sources, cycling, and impacts. *Chem. Rev.* **115**, 4035–4062 (2015).
15. Logan, J. A., Prather, M. J., Wofsy, S. C. & McElroy, M. B. Tropospheric chemistry: a global perspective. *J. Geophys. Res.: Oceans* **86**, 7210–7254 (1981).
16. Sherwen, T. et al. Global impacts of tropospheric halogens (Cl, Br, I) on oxidants and composition in GEOS-Chem. *Atmos. Chem. Phys.* **16**, 12239–12271 (2016).
17. Seinfeld, J. H. & Pandis, S. N. *Atmospheric Chemistry and Physics: From Air Pollution to Climate Change* (John Wiley & Sons, Hoboken, NJ, USA, 2016).
18. Gani, S. et al. Submicron aerosol composition in the world's most polluted megacity: the Delhi Aerosol Supersite study. *Atmos. Chem. Phys.* **19**, 6843–6859 (2019).
19. Pawar, P. V. et al. Chloride (HCl/Cl-) dominates inorganic aerosol formation from ammonia in the Indo-Gangetic Plain during winter: modeling and comparison with observations. *Atmos. Chem. Phys.* **23**, 41–59 (2023).
20. Sahoo, P. et al. What drives anthropogenic fine particulate chloride emissions in India?–A quantitative assessment of hotspots. *Sci. Total Environ.* **991**, 179949 (2025).
21. Zhang, B. et al. Global emissions of hydrogen chloride and particulate chloride from continental sources. *Environ. Sci. Technol.* **56**, 3894–3904 (2022).
22. Thamban, N. M. et al. Evolution of aerosol size and composition in the Indo-Gangetic Plain: size-resolved analysis of high-resolution aerosol mass spectra. *ACS Earth Space Chem.* **3**, 823–832 (2019).
23. Wang, X. et al. The role of chlorine in global tropospheric chemistry. *Atmos. Chem. Phys.* **19**, 3981–4003 (2019).
24. Sherwen, T. et al. Effects of halogens on European air-quality. *Faraday Discuss.* **200**, 75–100 (2017).
25. Sharma, G. et al. Gridded emissions of CO, NOx, SO2, CO2, NH3, HCl, CH4, $PM_{2.5}$, PM_{10}, BC, and NMVOC from open municipal waste burning in India. *Environ. Sci. Technol.* **53**, 4765–4774 (2019).
26. Fu, X. et al. Anthropogenic emissions of hydrogen chloride and fine particulate chloride in China. *Environ. Sci. Technol.* **52**, 1644–1654 (2018).
27. Yang, X. et al. The impact of chlorine chemistry combined with heterogeneous N2O5 reactions on air quality in China. *Atmos. Chem. Phys.* **22**, 3743–3762 (2022).
28. U.S. Environmental Protection Agency (EPA). National Emissions Inventory (NEI) Data https://www.epa.gov/air-emissions-inventories/2014-national-emissions-inventory-nei-data#datas Accessed: 24 September 2025 (2014).
29. Kuttippurath, J. et al. Record high levels of atmospheric ammonia over India: Spatial and temporal analyses. *Sci. Total Environ.* **740**, 139986 (2020).
30. Jayaraman, K. S. Indo-Gangetic Plains are ammonia hotspot of the world. *Nat. India* **740**, 139986 (2020).
31. Chen, Y. et al. Ammonium chloride associated aerosol liquid water enhances haze in Delhi, India. *Environ. Sci. Technol.* **56**, 7163–7173 (2022).
32. Keene, W. C. et al. Composite global emissions of reactive chlorine from anthropogenic and natural sources: Reactive Chlorine Emissions Inventory. *J. Geophys. Res.Atmos.* **104**, 8429–8440 (1999).
33. Liu, Y. et al. Modeling the impact of chlorine emissions from coal combustion and prescribed waste incineration on tropospheric ozone formation in China. *Atmos. Chem. Phys.* **18**, 2709–2724 (2018).
34. Haskins, J. D. et al. Wintertime gas-particle partitioning and speciation of inorganic chlorine in the lower troposphere over the Northeast United States and Coastal Ocean. *J. Geophys. Res. Atmos.* **123**, 12–897 (2018).
35. Tao, Y. et al. Hydrogen chloride (HCl) at ground sites during CalNex 2010 and insight into its thermodynamic properties. *J. Geophys. Res. Atmos.* **127**, e2021JD036062 (2022).
36. Acharja, P. et al. Thermodynamical framework for effective mitigation of high aerosol loading in the Indo-Gangetic Plain during winter. *Sci. Rep.* **13**, 13667 (2023).
37. Bondy, A. L. et al. Inland sea spray aerosol transport and incomplete chloride depletion: varying degrees of reactive processing observed during SOAS. *Environ. Sci. Technol.* **51**, 9533–9542 (2017).
38. Yang, L., Mukherjee, S., Pandithurai, G., Waghmare, V. & Safai, P. Influence of dust and sea-salt sandwich effect on precipitation chemistry over the Western Ghats during summer monsoon. *Sci. Rep.* **9**, 19171 (2019).
39. Nenes, A. et al. Aerosol acidity and liquid water content regulate the dry deposition of inorganic reactive nitrogen. *Atmos. Chem. Phys.* **21**, 6023–6033 (2021).
40. Osthoff, H. D. et al. High levels of nitryl chloride in the polluted subtropical marine boundary layer. *Nat. Geosci.* **1**, 324–328 (2008).

41. Roberts, J. M. et al. Laboratory studies of products of N2O5 uptake on Cl- containing substrates. *Geophys. Res. Lett.* **36**, L20808, 1–5 (2009).
42. Zhou, W. et al. Production of N2O5 and ClNO2 in summer in urban Beijing, China. *Atmos. Chem. Phys.* **18**, 11581–11597 (2018).
43. Hong, Y. et al. The role of anthropogenic chlorine emission in surface ozone formation during different seasons over eastern China. *Sci. Total Environ.* **723**, 137697 (2020).
44. Li, Q. et al. Impact of halogen chemistry on summertime air quality in coastal and continental Europe: application of the CMAQ model and implications for regulation. *Atmos. Chem. Phys.* **19**, 15321–15337 (2019).
45. Sarwar, G., Simon, H., Xing, J. & Mathur, R. Importance of tropospheric ClNO2 chemistry across the Northern Hemisphere. *Geophys. Res. Lett.* **41**, 4050–4058 (2014).
46. Sarwar, G., Simon, H., Bhave, P. & Yarwood, G. Examining the impact of heterogeneous nitryl chloride production on air quality across the United States. *Atmos. Chem. Phys.* **12**, 6455–6473 (2012).
47. Sarwar, G. & Bhave, P. V. Modeling the effect of chlorine emissions on ozone levels over the eastern United States. *J. Appl. Meteorol. Climatol.* **46**, 1009–1019 (2007).
48. Bharali, C., Nair, V. S., Chutia, L. & Babu, S. S. Modeling of the effects of wintertime aerosols on boundary layer properties over the Indo Gangetic Plain. *J. Geophys. Res. Atmos.* **124**, 4141–4157 (2019).
49. Xia, M. et al. Significant production of ClNO2 and possible source of Cl2 from N2O5 uptake at a suburban site in eastern China. *Atmos. Chem. Phys.* **20**, 6147–6158 (2020).
50. McCaslin, L. M., Götz, A. W., Johnson, M. A. & Gerber, R. B. Effects of microhydration on the mechanisms of hydrolysis and Cl- substitution in reactions of N2O5 and seawater. *ChemPhysChem* **24**, e202200819 (2023).
51. Riedel, T. P. et al. An MCM modeling study of nitryl chloride (ClNO2) impacts on oxidation, ozone production and nitrogen oxide partitioning in polluted continental outflow. *Atmos. Chem. Phys.* **14**, 3789–3800 (2014).
52. Wang, Z. et al. Fast heterogeneous N2O5 uptake and ClNO2 production in power plant and industrial plumes observed in the nocturnal residual layer over the North China Plain. *Atmos. Chem. Phys.* **17**, 12361–12378 (2017).
53. David, L. M. et al. Premature mortality due to $PM_{2.5}$ over India: Effect of atmospheric transport and anthropogenic emissions. *GeoHealth* **3**, 2–10 (2019).
54. Ghude, S. D. et al. Premature mortality in India due to $PM_{2.5}$ and ozone exposure. *Geophys. Res. Lett.* **43**, 4650–4658 (2016).
55. Bey, I. et al. Global modeling of tropospheric chemistry with assimilated meteorology: model description and evaluation. *J. Geophys. Res. Atmos.* **106**, 23073–23095 (2001).
56. Kim, P. S. et al. Sources, seasonality, and trends of southeast US aerosol: an integrated analysis of surface, aircraft, and satellite observations with the GEOS-Chem chemical transport model. *Atmos. Chem. Phys.* **15**, 10411–10433 (2015).
57. Pai, S. J. et al. An evaluation of global organic aerosol schemes using airborne observations. *Atmos. Chem. Phys.* **20**, 2637–2665 (2020).
58. David, L. M. et al. Tropospheric ozone over the Indian subcontinent from 2000 to 2015: data set and simulation using GEOS-Chem chemical transport model. *Atmos. Environ.* **219**, 117039 (2019).
59. Lu, X. et al. Lower tropospheric ozone over India and its linkage to the South Asian monsoon. *Atmos. Chem. Phys.* **18**, 3101–3118 (2018).
60. Malasani, C. R. et al. Modeling of mercury deposition in India: evaluating emission inventories and anthropogenic impacts. *Environ. Sci. Processes Impacts*https://doi.org/10.1039/D4EM00324A (2024).
61. Anchan, N. L. et al. Assessing the variability of Aerosol Optical Depth over India in response to future scenarios: Implications for carbonaceous aerosols. *J. Geophys. Res. Atmos.* **129**, e2024JD040846 (2024).
62. Bertram, T. & Thornton, J. Toward a general parameterization of N2O5 reactivity on aqueous particles: the competing effects of particle liquid water, nitrate and chloride. *Atmos. Chem. Phys.* **9**, 8351–8363 (2009).
63. Eastham, S. D., Weisenstein, D. K. & Barrett, S. R. Development and evaluation of the unified tropospheric–stratospheric chemistry extension (UCX) for the global chemistry-transport model GEOS-Chem. *Atmos. Environ.* **89**, 52–63 (2014).
64. Keller, C. et al. HEMCO v1. 0: a versatile, ESMF-compliant component for calculating emissions in atmospheric models. *Geosci. Model Dev.* **7**, 1409–1417 (2014).
65. Guenther, A. et al. Estimates of global terrestrial isoprene emissions using MEGAN (Model of Emissions of Gases and Aerosols from Nature). *Atmos. Chem. Phys.* **6**, 3181–3210 (2006).
66. Giglio, L., Randerson, J. T. & Van Der Werf, G. R. Analysis of daily, monthly, and annual burned area using the fourth-generation global fire emissions database (GFED4). *J. Geophys. Res. Biogeosci.* **118**, 317–328 (2013).
67. Singh, A., Satish, R. V. & Rastogi, N. Characteristics and sources of fine organic aerosol over a big semi-arid urban city of western India using HR-ToF-AMS. *Atmos. Environ.* **208**, 103–112 (2019).
68. Haslett, S. L. et al. Nighttime NO emissions strongly suppress chlorine and nitrate radical formation during the winter in Delhi. *Atmos. Chem. Phys.* **23**, 9023–9036 (2023).
69. Gong, S. A parameterization of sea-salt aerosol source function for sub- and super-micron particles. *Global Biogeochem. Cycles* **17,** 1097, 1–7 (2003).
70. Jaeglé, L., Quinn, P., Bates, T., Alexander, B. & Lin, J.-T. Global distribution of sea salt aerosols: new constraints from in situ and remote sensing observations. *Atmos. Chem. Phys.* **11**, 3137–3157 (2011).
71. Zhu, L. et al. Effect of sea salt aerosol on tropospheric bromine chemistry. *Atmos. Chem. Phys.* **19**, 6497–6507 (2019).

Acknowledgements

A.P. thank the DST-INSPIRE Fellowship (2020/IF200113/SP23241491CE). We acknowledge the computational support provided by the Max Planck Computing and Data Facility (MPCDF). We thank Central Pollution Control Board (CPCB) for the publicly available data (https://cpcb.nic.in/) and Ms. Anu M. for compiling the data and further analysis. We are grateful to all the team members of HACPL (IITM, Pune) for providing pCl– data. Authors sincerely thank the two anonymous reviewers for their careful reading of the manuscript providing, constructive suggestions and valuable inputs, which helped us improve the quality and clarity of our manuscript.

Author contributions

S.S.G. conceived the research idea and A.P. independently set up the GEOS-Chem model to study the research idea with support from C.R., and P.L.; A.P., and B.Z. carried out the assessment of HCl emission inventory for further use in GEOS-Chem model for use over Indian region. A.P. independently carried out the comprehensive model simulations, data analyses, and plotting. A.P. carried out scientific interpretation in consultation with P.L., S.S.G., and S.T.M.; A.P. wrote the first draft and led manuscript development under the supervision of S.S.G. with contributions from G.P., B.S., and P.L. Critical inputs and further valuable edits to the manuscript were provided by S.T.M. and M.O.A.; The manuscript was read and approved by all contributing authors.

Competing interests

Sachin S. Gunthe is an Associate Editor of npj Clean Air, and he was not involved in the journal's review of, or decisions related to, this manuscript. The remaining authors declare no competing interests.

Additional information

Supplementary information The online version contains supplementary material available at https://doi.org/10.1038/s44407-026-00066-5.

Correspondence and requests for materials should be addressed to Ankit Patel or Sachin S. Gunthe.